**World Journal of Nano Science and Engineering, 2016, 6, 1-19**
Published Online March 2016 in SciRes. http://www.scirp.org/journal/wjnse
http://dx.doi.org/10.4236/wjnse.2016.61001

# Sol-Gel Synthesis Using Novel Chelating Agent and Electrochemical Characterization of Binary Doped $LiMn_2O_4$ Spinel as Cathode Material for Lithium Rechargeable Batteries

**Ramasamy Thirunakaran[1*], Gil Hwan Lew[2], Won-Sub Yoon[2*]**

[1]CSIR-Central Electrochemical Research Institute, Karaikudi, India
[2]Department of Energy Science, Sungkyunkwan University, Suwon, Republic of Korea
Email: *rthirunakaran@yahoo.com, *wsyoon@skku.edu

Received 2 November 2015; accepted 12 January 2016; published 15 January 2016



## Abstract

**$LiMn_2O_4$ and $LiCu_xCr_yMn_{2-x-y}O_4$ (x = 0.50; y = 0.05 - 0.50) powders have been synthesized via sol-gel method for the first time using Myristic acid as chelating agent. The synthesized samples have been taken to physical and electrochemical characterization such as thermo gravimetric analysis (TG/DTA), X-ray diffraction (XRD), Fourier transform infrared spectroscopy (FT-IR), field-emission scanning electron microscopy (FESEM), transmission electron microscopy (TEM) and electrochemical characterization *viz.*, electrochemical galvanostatic cycling studies, electrochemical impedance spectroscopy (EIS) and differential capacity curves (dQ/dE). XRD patterns of $LiMn_2O_4$ and $LiCu_xCr_yMn_{2-x-y}O_4$ confirm high degree of crystallinity with good phase purity. FESEM image of undoped pristine spinel lucidly depicts cauliflower morphology with good agglomerated particle size of 50 nm while 0.5-Cu doped samples depict the pebbles morphology. TEM images of the spinel $LiMn_2O_4$ and $LiCu_{0.5}Cr_{0.05}Mn_{1.45}O_4$ authenticate that all the synthesized particles via sol-gel method are nano-sized (100 nm) with spherical surface and cloudy particles morphology. The $LiMn_2O_4$ samples calcined at 850˚C deliver the high discharge capacity of 130 mA·h/g with cathodic efficiency of 88% corresponds to 94% columbic efficiency in the first cycle. Among all four compositions studied, $LiCu_{0.5}Cr_{0.05}Mn_{1.45}O_4$ delivers 124 mA·h/g during the first cycle and shows stable performance with a low capacity fade of 1.1 mA·h/g cycle over the investigated 10 cycles.**

## Keywords

**Multi-Doping, Sol-Gel Method, Myristic Acid, Differential Capacity, Spinel Cathode**

*Corresponding authors.

**How to cite this paper:** Thirunakaran, R., Lew, G.H. and Yoon, W.-S. (2016) Sol-Gel Synthesis Using Novel Chelating Agent and Electrochemical Characterization of Binary Doped $LiMn_2O_4$ Spinel as Cathode Material for Lithium Rechargeable Batteries. *World Journal of Nano Science and Engineering*, **6**, 1-19. http://dx.doi.org/10.4236/wjnse.2016.61001

## 1. Introduction

Spinel $LiMn_2O_4$ has been zeroed in attractive and promising cathode materials for lithium-ion batteries owing to its high voltages, proper $Mn^{3+}/Mn^{4+}$ redox potential, high energy densities and high power densities. Lithium-ion batteries are much dependent on cathode material insertion-deinsertion processes. $LiMn_2O_4$, $LiCoO_2$ are used as commercial positive cathode materials for various applications and high-voltage spinel cathode materials are also used for various energy-storage devices. Among all the positive materials used for lithium-ion battery applications, $LiMn_2O_4$ is an apt cathode material for rechargeable lithium-ion batteries, owing to its low cost, easy availability, environmentally benign nature, non-toxicity, and ease of synthesis while comparing with other layered oxides such as $LiCoO_2$ and $LiNiO_2$ [1]-[3]. However, specific capacity of undoped $LiMn_2O_4$ decreases gradually upon repeated cycling carried out at elevated temperature [4] [5]. It is well known that the capacity fading is caused due to several factors such as Jahn-Teller distortion, two-phase unstable reaction [2], slow dissolution of manganese into the electrolyte [6], lattice instability [7], and particle size distribution [8] [9]. In order to overcome the problem of Jahn-Teller distortion for obtaining the high capacity retention, several researchers have investigated earlier lithium rich spinels with various divalent, trivalent and tetravalent-doped ions such as Cr, Fe, Zn, Cu, Ga, Co, Al, Ni and Ti [10]. Ohzuku *et al*. [8] and Lee *et al*. [11] showed that partial doping of cations is effective in suppressing the capacity fade upon cycling. Moreover, the capacity fade of $LiMn_2O_4$ often happens much in 3 V region which can be completely suppressed by doping selenium with $LiMn_2O_4$ [12]. Low temperature synthesis methods *viz.*, sol-gel [13] [14], chemical precipitation [15], hydrothermal and pechini process [16] have been used to obtain cathode materials with expected physical and electrochemical properties to use in lithium-ion batteries. Spinel $LiMn_2O_4$ and Zn, Co, Ni and substituted $LiMn_2O_4$ synthesized via facile sol-gel method to improve the electrochemical and structural properties of $LiMn_2O_4$ spinel based on electrode materials for Li-ion batteries [17]. The present work highlights that efforts have been taken to synthesize physical and electrochemical characterization of $LiMn_2O_4$ and $LiCu_xCr_yMn_{2-x-y}O_4$ (x = 0.50; y = 0.05 - 0.50) via sol-gel method using Myristic acid as new chelating agent for the exploration of this facile synthesis method with good electrochemical performance.

## 2. Experimental

$LiMn_2O_4$ and $LiCu_xCr_yMn_{2-x-y}O_4$ (x = 0.50; y = 0.05 - 0.50) powders have been synthesized via sol-gel method using Myristic acid as chelating agent. **Figure 1** depicts the flow chart of the synthesis procedure. Stoichiometric amounts of acetates of lithium, manganese, and the dopant salts such as acetate of copper and chromium were dissolved independently in triple-distilled water. The chelating agent (Myristic acid) is dissolved slowly in heating ethyl alcohol gently. After dissolving all the salts gently, it will be mixed with chelating agent. A small amount of precursor has been taken for TG/DTA analysis to under the thermal behaviour and the rest of the sample is calcined at 850˚C for 6 h. For thermal analysis, the precursors are heated in air atmosphere at 10˚C/min to 850˚C. All the calcined samples are subjected for physical characterization using thermo gravimetric/differential thermal analysis (TG/DTA-Seiko Exstart 6000, Japan), X-ray diffraction (XRD-Bruker D2 Phaser desktop, Cu source, AXS, Karisruhe, Germany), Fourier-transform infrared spectroscopy (FTIR-Tensor 27, Bruker (Germany)), field emission scanning electron microscopy (FESEM-JEOL, Model-JSM-7000F (Japan)), transmission electron microscopy (TEM-JEOL, JEM-ARM 200F, Japan), energy dispersive X-ray analysis (EDAX-JEOL, Model-JSM-7000F, Japan) and galvanostatic charge-discharge cycling studies (WonATech-Model, WBCS 3000, South Korea), electrochemical impedance spectroscopy (EIS-Potentiostat/Galva-nostat, Model-273A, USA) and differential capacity curves (dQ/dE).

### Electrochemical Studies

Coin cells of 2032 configuration have been assembled in an argon filled glove box (MBraun, Germany) using lithium foil as anode, Celgard 2400 as separator, 1 M solution of $LiPF_6$ and 0.3 M $LiBF_4$ in 3:7 (v/v) volume mixture of ethylene carbonate (EC) and diethyl carbonate (DEC) as electrolyte and the synthesized material has been as cathode. The cathode is prepared by slurry coating procedure from a mix comprising synthesized compound, Super P carbon black as conducting material and poly (vinylidiene fluoride) 5% PVdF binder in *n*-methyl-2-pyrrolidone (NMP) solution mixed in the percentage ratio of 80:10:10 so as to form slurry. The slurry has been coated over aluminum foil and vacuum dried at 110˚C for 2 h. Electrode blanks of 18 mm diameter

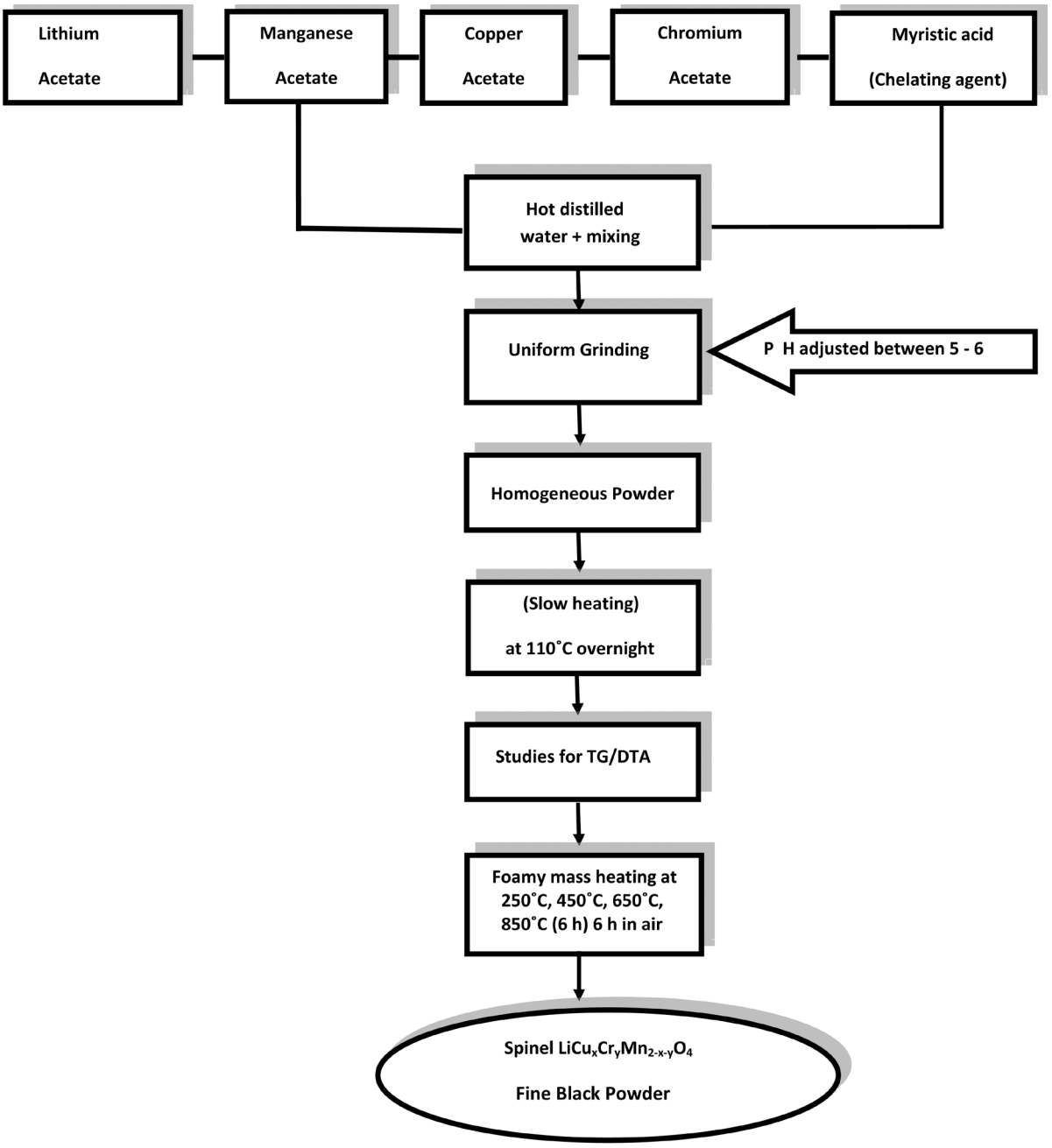


**Figure 1.** Flow chart for synthesis of $LiCu_xCr_yMn_{2-x-y}O_4$ by sol-gel method using Myristic acid as chelating agent.

are punched out and used as cathode in the coin cell. The fabricated 2032 coin cells have been cycled at a constant current of C/10 rate between 3.0 to 4.5 V using an in-house battery cycling unit.

## 3. Results and Discussion

### 3.1. Thermal Studies

The TG/DTA curve of $LiMn_2O_4$ precursor is depicted in **Figure 2(a)**. The TGA curve clearly illustrates the three weight loss regions. *Ab initio*, the low weight loss of 5% is seen up to 100˚C owing to removal of water. Further, another two regions are observed between 100 V and 350˚C extending with maximum weight loss of 45% may be assigned to the decomposition of chelating agent (Myristic acid) and acetate precursors. It is well known that

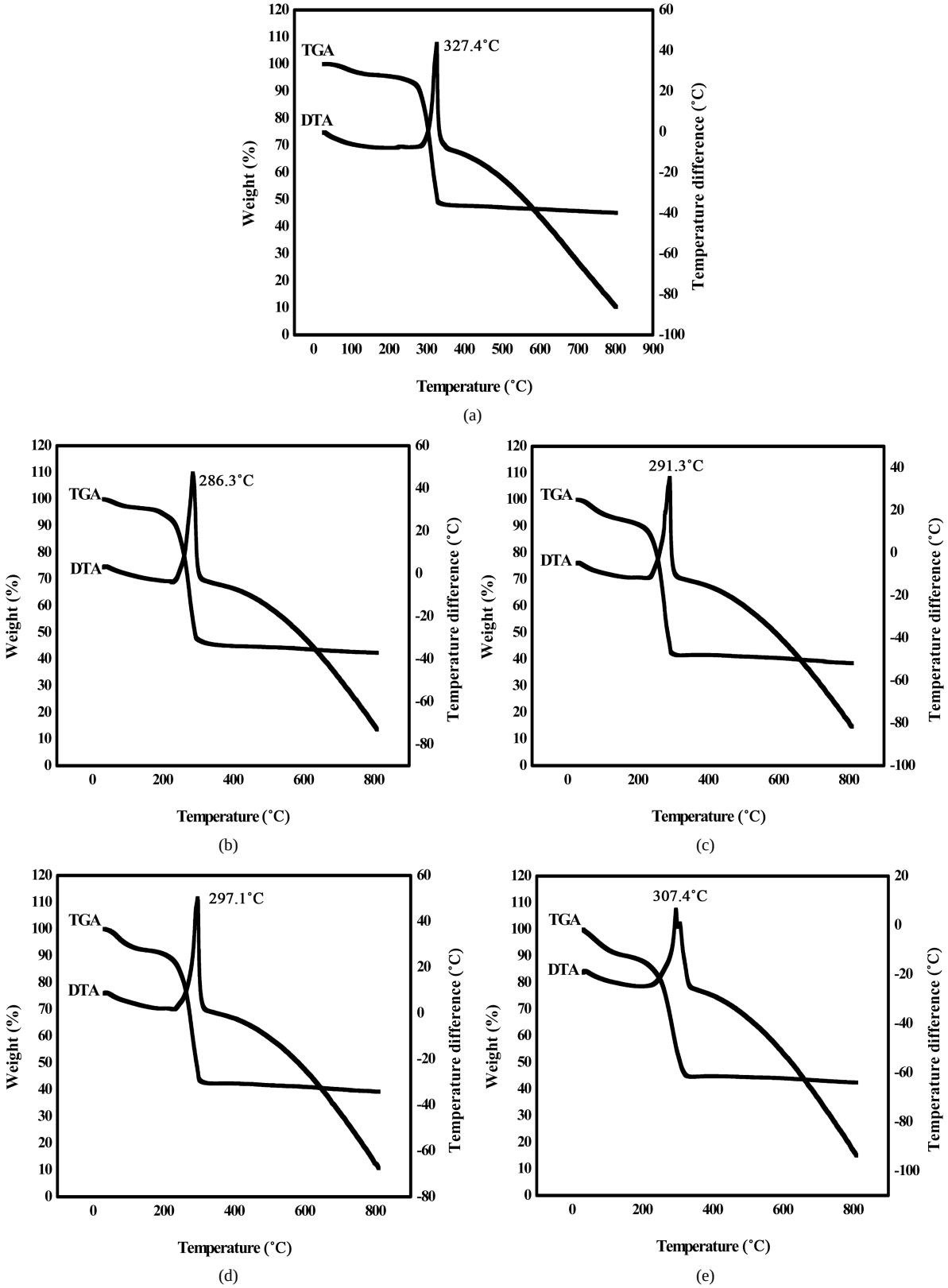


**Figure 2.** Thermo gravimetric and differential thermal analysis (TG/DTA) of $LiMn_2O_4$ and $LiCu_xCr_vMn_{2-x-v}O_4$ spinel precursor. (a) Undoped; (b) Cu: 0.50; (c) Cu: 0.50; Cr: 0.05; (d) Cu: 0.50; Cr: 0.10 and (e) Cu: 0.50; Cr: 0.50.

in the case of DTA curve, it depicts lucidly a well defined exothermic peak at 327.4˚C indicating the formation of the spinel compound which is mirrored in the XRD pattern corresponding to high degree of crystallinity for the sample calcined at 850˚C. Furthermore, all the peak reflections of $LiMn_2O_4$ have been shown unclouded when the precursor is calcined at 250˚C and 450˚C. Also, the TGA curve shows that the temperature above 350˚C stops totally thermal events without any further thermal reaction after the formation of spinel compounds.

TG/DTA curves of spinel $LiCu_xCr_yMn_{2-x-y}O_4$ (x = 0.50; y = 0.05 - 0.50) precursors have been synthesized via sol-gel method using Myristic acid as chelating agent are presented in **Figures 2(b)-(e)**. TGA curve of copper doped spinel precursor shows three characteristic weight loss zones (**Figure 2(b)**). Initially, the low weight loss of 5% up to 100˚C is an account of removal of moisture. The second and third weight loss zone of 40% up to 300˚C is attributed to the decomposition of acetate precursor of copper. DTA curve shows a well defined an exothermic peak at 286.3˚C suggesting the formation of spinel product. DTA curve corroborates no further thermal reactions are taking place beyond 300˚C.

Moreover, in the case of dual doped spinel ($LiCu_xCr_yMn_{2-x-y}O_4$) precursor, $LiCu_{0.5}Cr_{0.05}Mn_{1.45}O_4$ shows the same three weight loss zones with weight loss of 5% compared to other all dual dopant concentration of the spinel precursors. This low amount in weight loss has been reflected in charge-discharge study to deliver the high discharge capacity of the spinel. Among all dual doped spinel precursors, equal doping ratio or Cu-Cr high doping of $LiCu_{0.5}Cr_{0.5}MnO_4$, shows a well defined exothermic peak (see **Figure 2(e)**) at 307.4˚C with higher formation temperature owing to higher specific heat of Cr than Cu and Mn (Cr = 0.46 kJ/kg K; Cu = 0.39 kJ/kg K; Mn = 0.48 kJ/kg K).

Hence, in all cases, the weight loss zones complete up to 100˚C may be attributed to the removal of moisture and resulting in the formation of spinel at around 307.4˚C - 327.4˚C. This temperature difference (20˚C) is depicted in the formation temperature of all doped precursors which leads the reaction to begin much earlier and involving higher heat energy (307.4˚C) as indicated in the DTA curve (**Figure 2(e)**). All precursors show lucidly thermally inactive regions beyond 300˚C indicating the closure of thermal events.

## 3.2. X-Ray Diffraction Studies

**Figures 3(a)-(e)** depicts the XRD patterns of $LiMn_2O_4$ samples calcined at different temperatures: (a) as synthesized; (b) 250˚C; (c) 450˚C; (d) 650˚C; (e) 850˚C. It is evident that as synthesized and the samples calcined at 250˚C exhibits broad and indistinct reflections indicating the nebulous nature of the compounds. Moreover, the sample calcined at 450˚C and 650˚C exhibits an additional impurity peaks may be attributed to the formation of $\alpha$-$Mn_2O_3$ and $LiMn_2O_3$. Similarly, the high intensity peaks such as (111), (311), (222), (400), (331), (551), (440) and (351) have been obtained for the samples calcined at 850˚C for 6 h confirms the high degree of crystallinity with better phase purity. These planes are in good agreement with the results obtained for the spinel compound synthesized via sol-gel method or solid-state method [17]-[26]. It is well known that the spinel compound has an Fd3m space group wherein lithium occupies at 8a tetrahedral sites, manganese and dopant ions occupy the

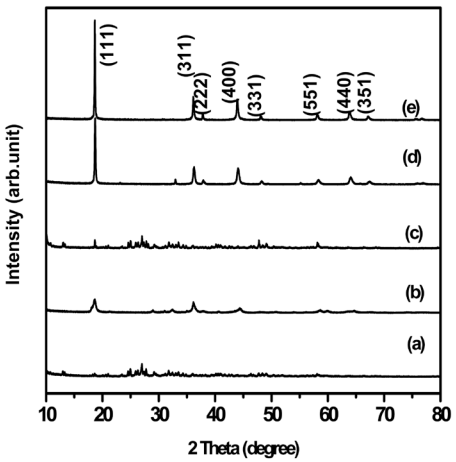


**Figure 3.** XRD patterns of sol-gel-synthesized undoped $LiMn_2O_4$ samples calcined at different temperatures *viz.*, (a) As synthesized; (b) 250˚C; (c) 450˚C; (d) 650˚C; and (e) 850˚C.

16d sites and oxygen at 32e sites. All the XRD peak reflections for synthesized spinel match perfectly with Joint committee on Powder Diffraction Standard (JCPDS card No. 35-782).

The XRD patterns of $LiCu_xCr_yMn_{2-x-y}O_4$ are shown in **Figures 4(a)-(d)** with different stoichiometric amounts of divalent and trivalent metal cations *viz*., Cu and Cr (Cu-0.5; Cr-0.05-0.5), synthesized via sol-gel method calcined at 850˚C. $LiMn_2O_4$ and $LiCu_xCr_yMn_{2-x-y}O_4$ depict the formation of phase pure crystalline spinels in substantiating the first order reaction. Moreover, it is clear that all the peaks corresponding to (111), (311), (222), (400), (331), (551), (440) and (351) which are in good accordance with other researchers [24]. All the XRD peak reflections for this pristine spinel perfectly match with Joint committee on Powder Diffraction Standard (JCPDS card No. 35-782).

## 3.3. FTIR Spectroscopy

The FT-IR spectra of sol-gel synthesized $LiMn_2O_4$ powders calcined at different temperatures *viz*., 250˚C, 450˚C, 650˚C and 850˚C are shown in **Figures 5(a)-(d)**. It is clear that the broad peaks appear for the sample calcined at low temperature (250˚C, 450˚C and 650˚C) for the sake of the water molecules (O-H bond). FT-IR studies on $LiAl_xMn_{2-x}O_4$ have been investigated through solid-state combustion synthesis method in which all the frequencies showing striking similarity with our present investigation [27]. It is ratified that in the case of black coloured spinel compound obtained via sol-gel method exhibiting the two IR spectral bands at wavelengths between 513 - 516 $cm^{-1}$ and 607 - 610 $cm^{-1}$ for the sample calcined at 850˚C could be assignable to the Li-O bending vibration mode and Li-Mn-O stretching vibration band. The sample calcined at low temperature (250˚C) depicting the low wave number while comparing to undoped spinel calcined at 850˚C. The wave number corresponding to the $LiMn_2O_4$ and $LiCu_xCr_yMn_{2-x-y}O_4$ spinels are given in **Table 1** and **Table 2**. Also, the sample calcined at 850˚C depicts the IR band at around 610 $cm^{-1}$ which is slightly shifted towards the lower wave number.

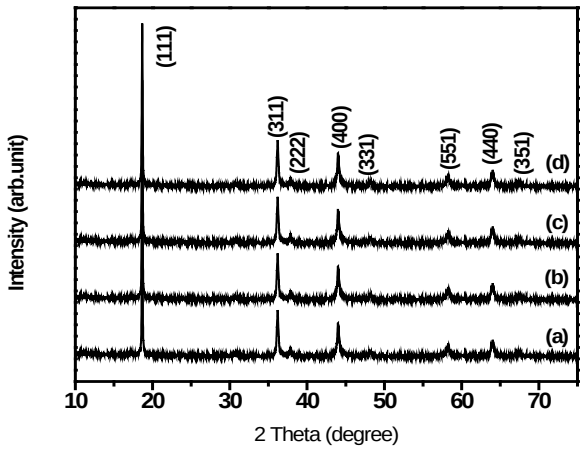


**Figure 4.** XRD patterns of $LiCu_xCr_yMn_{2-x-y}O_4$ powders calcined at 850˚C. (a) Cu: 0.50; (b) Cu: 0.50; Cr: 0.05; (c) Cu: 0.50; Cr: 0.10 and (d) Cu: 0.50; Cr: 0.50.

**Table 1.** FTIR frequencies for the peaks observed for $LiMn_2O_4$.

| No | Temperature | Wave number ($cm^{-1}$) | Assignments |
|---|---|---|---|
| 1 | 250 | 513 | Li-O |
| | | 607 | Li-Mn-O |
| 2 | 450 | 505 | Li-O |
| | | 613 | Li-Mn-O |
| 3 | 650 | 516 | Li-O |
| | | 619 | Li-Mn-O |
| 4. | 850 | 516 | Li-O |
| | | 610 | Li-Mn-O |

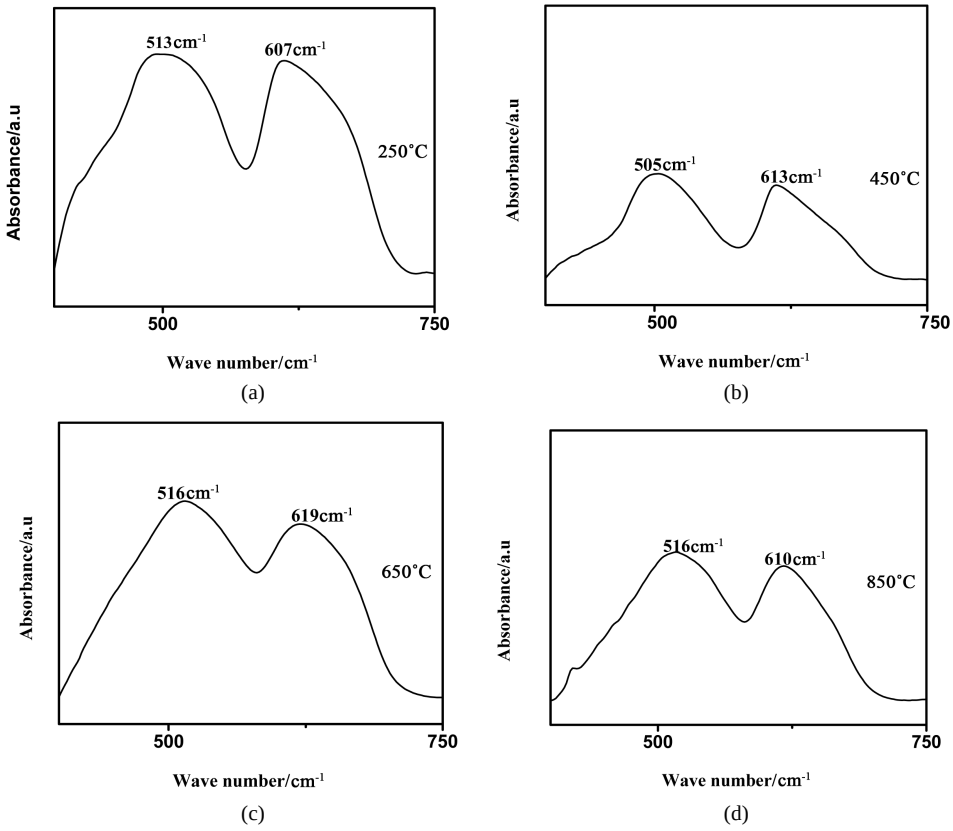


**Figure 5.** FT-IR spectra of spinel $LiMn_2O_4$ (a)-(d) particles calcined at different temperatures *viz.*, 250˚C, 450˚C, 650˚C and 850˚C.

**Table 2.** FTIR frequencies for the peaks observed for $LiCu_xCr_yMn_{2-x-y}O_4$.

| No | Sample | Wave number ($cm^{-1}$) | Assignments |
|---|---|---|---|
| 1 | $LiCu_{0.5}Mn_{1.5}O_4$ | 523 | Li-O |
| | | 625 | Li-Cu-Mn-O |
| 2 | $LiCu_{0.5}Cr_{0.05}Mn_{1.45}O_4$ | 505 | Li-O |
| | | 621 | Li-Cu-Cr-Mn-O |
| 3 | $LiCu_{0.5}Cr_{0.10}Mn_{1.40}O_4$ | 503 | Li-O |
| | | 618 | Li-Cu-Cr-Mn-O |
| 4 | $LiCu_{0.5}Cr_{0.5}Mn_{1.0}O_4$ | 525 | Li-O |
| | | 625 | Li-Cu-Cr-Mn-O |

**Figures 6(a)-(d)** depict the FT-IR spectra of $LiCu_xCr_yMn_{2-x-y}O_4$powders with varying amounts of Cu and Cr. It is clearly shown that the di and trivalent doped spinels exhibiting the two IR spectral bands between 523 - 525 $cm^{-1}$ and 618 - 625 $cm^{-1}$ may be attributed to the Li–O bending vibration at lower wave number and Li-Cu-Cr-Mn-O stretching vibration at higher wave number respectively. The FT-IR on $LiCr_xNi_yMn_{2-x-y}O_4$ reveals the synthesis process via sol-gel method [28]. These results are is in good agreement with our FTIR data. Similarly, $LiCr_xCu_yMn_{x-y}O_4$ has been synthesized via wet chemistry method and reveals the spectra of stretching and bending vibration [29]. Such reports show the striking similarity in our present investigation. Nevertheless, it is corroborated that there are no any significant impurity peak reflections in all samples were calcined at 850˚C. High equal amount of dual doping spinel ($LiCu_{0.5}Cr_{0.5}MnO_4$) exhibits the spectral bands 525 $cm^{-1}$ and 625 $cm^{-1}$ which is similar to wave number of 0.5-Cu doped spinel.

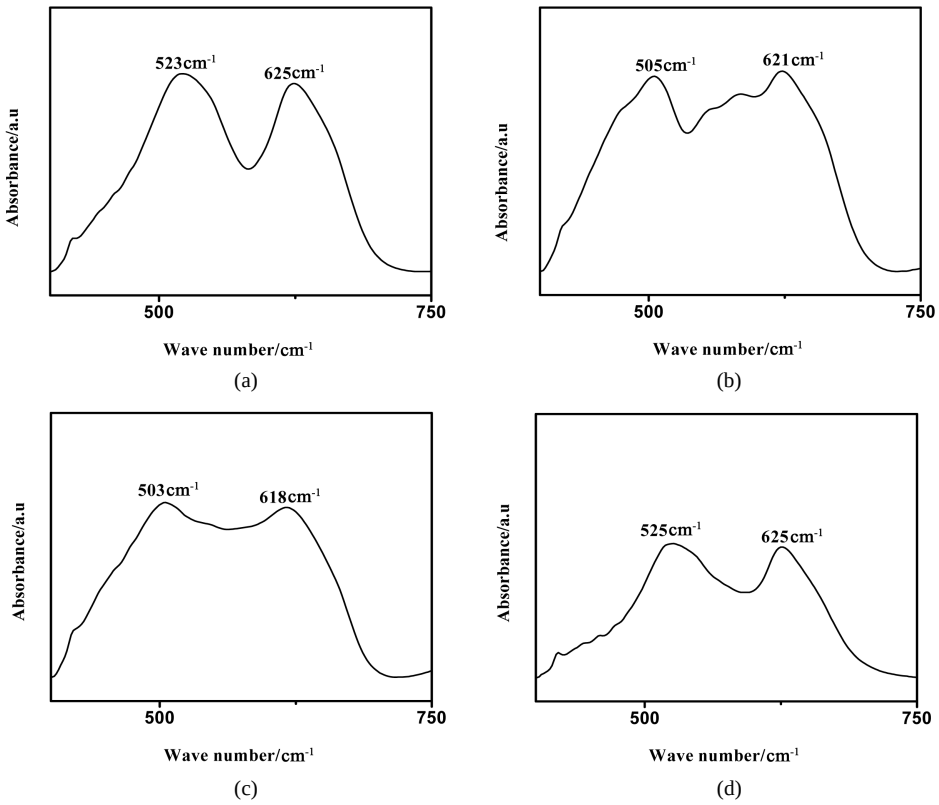


**Figure 6.** FT-IR spectra of $LiCu_xCr_yMn_{2-x-y}O_4$ particles with varying Cu-Cr doping calcined at 850˚C. (a) x = 0.50; (b) x = 0.50; y = 0.05; (c) x = 0.50; y = 0.10; (d) x = 0.50; y = 0.50.

## 3.4. FESEM Analysis

**Figures 7(a)-(e)** depict the Field Emission Scanning Electron Microscope images of undoped and $LiCu_xCr_yMn_{2-x-y}O_4$ spinel powders calcined at 850˚C. The undoped pristine spinel depicts cauliflower morphology with an average particle size of 50 nm (**Figure 7(a)**) with good agglomerated particles. Similarly in the case of Cu doped samples, it is lucidly seen pebbles morphology seems to be 2 µm. It is evident that 0.05-Cr (**Figure 7(c)**) doped spinel depicts spherical surface morphology with less particle size of 0.50 µm. The equal doping ratio of $LiCu_{0.50}Cr_{0.50}Mn_{1.0}O_4$ shows clearly that all the large particles are seen to be spherical grains haphazardly with an increased particle size of 2 µm as it possesses high amount of Cu-Cr doping which is reflected in electrochemical impedance spectroscopy (EIS) and cycling behavior of the doped spinel.

## 3.5. TEM Analysis

**Figures 8(a)-(f)** depict the TEM images of $LiMn_2O_4$ and $LiCu_xCr_yMn_{2-x-y}O_4$ particles calcined at 850˚C. **Figure 8(a)** illustrates the selected area of diffraction pattern ($LiMn_2O_4$) suggesting the diffuse hollow with multiple fringes. The undoped spinel shows (**Figure 8(b)**) uniform spherical morphology with particle size of (100 nm). In the case of $LiCu_{0.5}Mn_{1.5}O_4$, (**Figure 8(c)**) all the particles are seen like large spherical surface morphology. Moreover, $LiCu_{0.5}Cr_{0.05}Mn_{1.45}O_4$ (**Figure 8(d)**), depicts cloudy particles with good agglomerated particle size of 100 nm. This good agglomeration has been lucidly resulted to increase the high the electrochemical activity of the spinel among all dopants. Therefore, the high equal amount of dual doping spinel ($LiCu_{0.5}Cr_{0.5}MnO_4$) (**Figure 8(f)**) depicts the typical morphology with large particles since chromium content is higher than that of other dopant which is unclouded reflected in charge-discharge studies leading to rapid capacity fading upon the cycling.

## 3.6. EDAX Analysis

**Figures 9(a)-(e)** depict the EDAX peaks of Cu, Cr, Mn and O in $LiMn_2O_4$ and $LiCu_xCr_yMn_{2-x-y}O_4$ compounds.

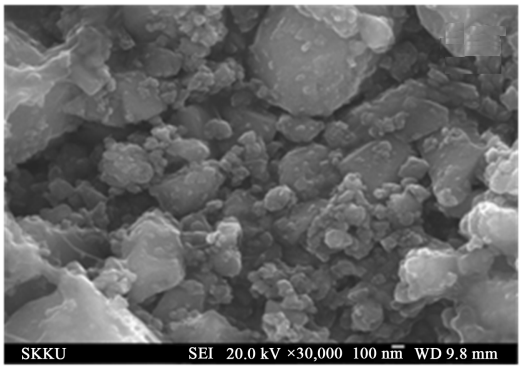


(a)

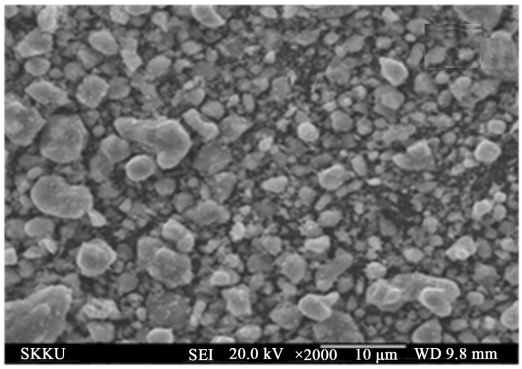


(b)

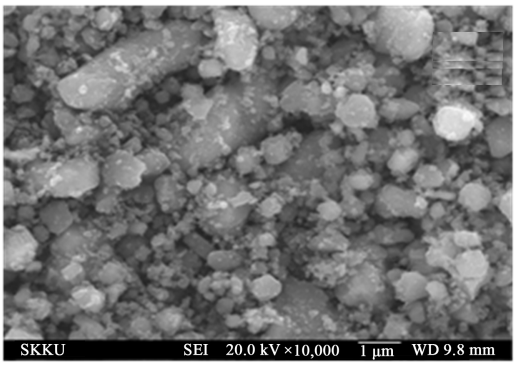


(c)

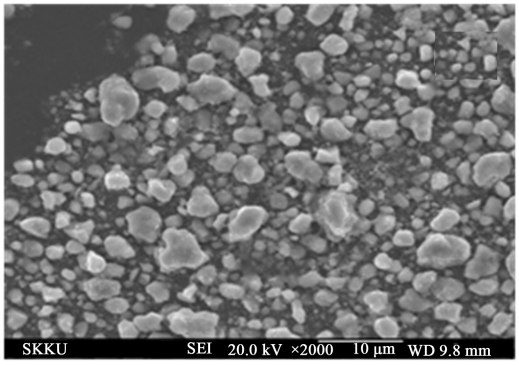


(d)

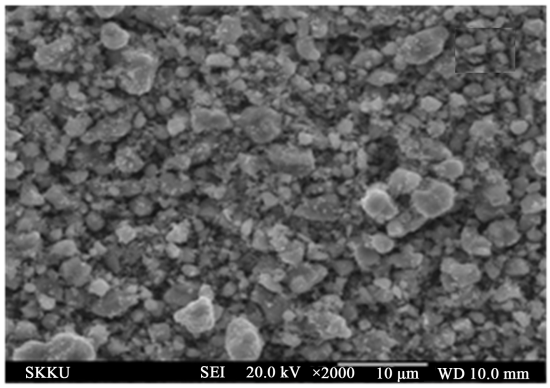


(e)

**Figure 7.** FESEM images of spinel $LiMn_2O_4$ and $LiCu_xCr_vMn_{2-x-v}O_4$ particles calcined at 850˚C. (a) Undoped; (b) Cu: 0.50; (c) Cu: 0.50; Cr: 0.05, (d) Cu: 0.50; Cr: 0.10 and (e) Cu: 0.50; Cr: 0.50.

All the EDAX peaks corroborate lucidly the actual compositions of the undoped and doped spinels to be pure without any additional impurities. **Table 3** depicts the EDAX compositions of various elements in $LiMn_2O_4$ and $LiCu_xCr_yMn_{2-x-y}O_4$.

## 3.7. Galvanostatic Charge-Discharge Studies

**Figures 10(a)-(e)** show the first cycle charge-discharge behavior of $LiMn_2O_4$ and $LiCu_xCr_yMn_{2-x-y}O_4$ with different stoichiometric concentration of Cu and Cr. The charge-discharge behavior of undoped and $LiCu_xCr_yMn_{2-x-y}O_4$ shows pellucid the de-intercalation/intercalation of lithium ions at the 8a tetrahedral sites from cubic spinel structure. At the beginning, $LiMn_2O_4$ has been synthesized via sol-gel method and calcined at 850˚C delivers the high discharge capacity of 130 mA·h/g against the charging capacity of 138 mA·h/g with

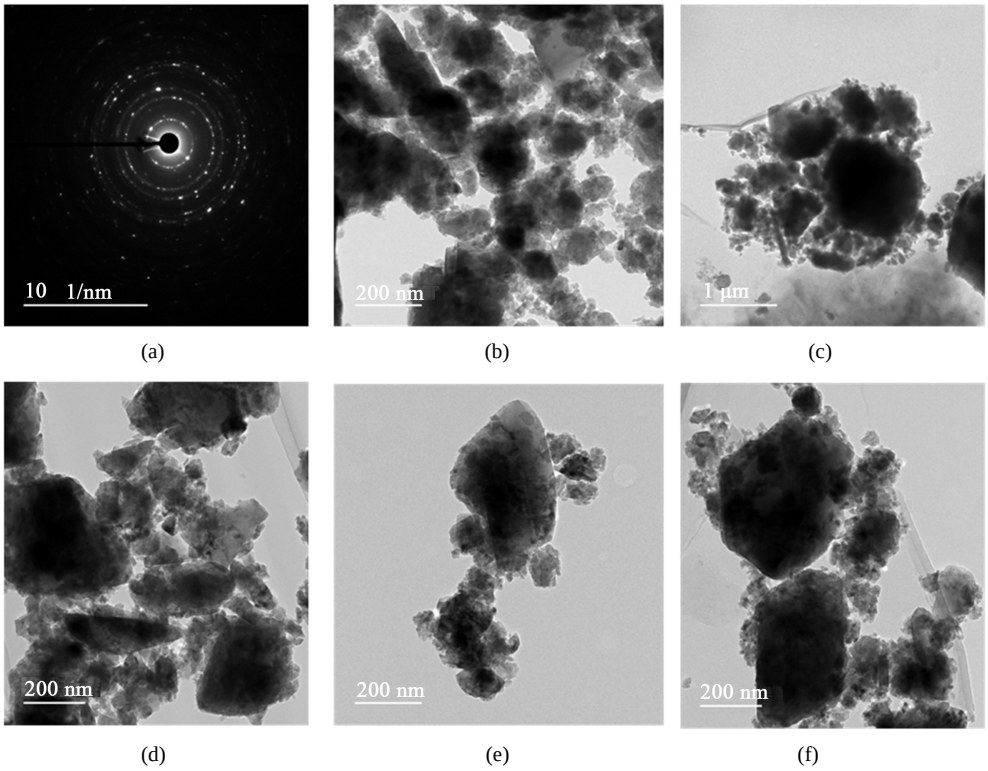


**Figure 8.** TEM images of $LiMn_2O_4$ and $LiCu_xCr_vMn_{2-x-v}O_4$ particles calcined at 850˚C. (a) (b) Undoped; (c) Cu: 0.50; (d) Cu: 0.50; Cr: 0.05; (e) Cu: 0.50; Cr: 0.10 and (f) Cu: 0.50; Cr: 0.50.

**Table 3.** EDAX compositions of various elements in $LiMn_2O_4$ and $LiCu_xCr_yMn_{2-x-y}O_4$.

| Element | Name of the compound | Weight % |
|---|---|---|
| | $LiMn_2O_4$ | |
| O | | 34.02 |
| Mn | | 65.98 |
| | $LiCr_{0.5}Mn_{1.5}O_4$ | |
| O | | 28.25 |
| Mn | | 53.50 |
| Cr | | 18.25 |
| | $LiCr_{0.5}Cu_{0.05}Mn_{1.45}O_4$ | |
| O | | 26.45 |
| Mn | | 49.75 |
| Cr | | 17.12 |
| Cu | | 6.21 |
| | $LiCr_{0.5}Cu_{0.10}Mn_{1.40}O_4$ | |
| O | | 27.19 |
| Mn | | 47.15 |
| Cr | | 16.41 |
| Cu | | 9.25 |
| | $LiCr_{0.5}Cu_{0.50}Mn_{1.0}O_4$ | |
| O | | 25.75 |
| Mn | | 46.95 |
| Cr | | 16.55 |
| Cu | | 10.75 |

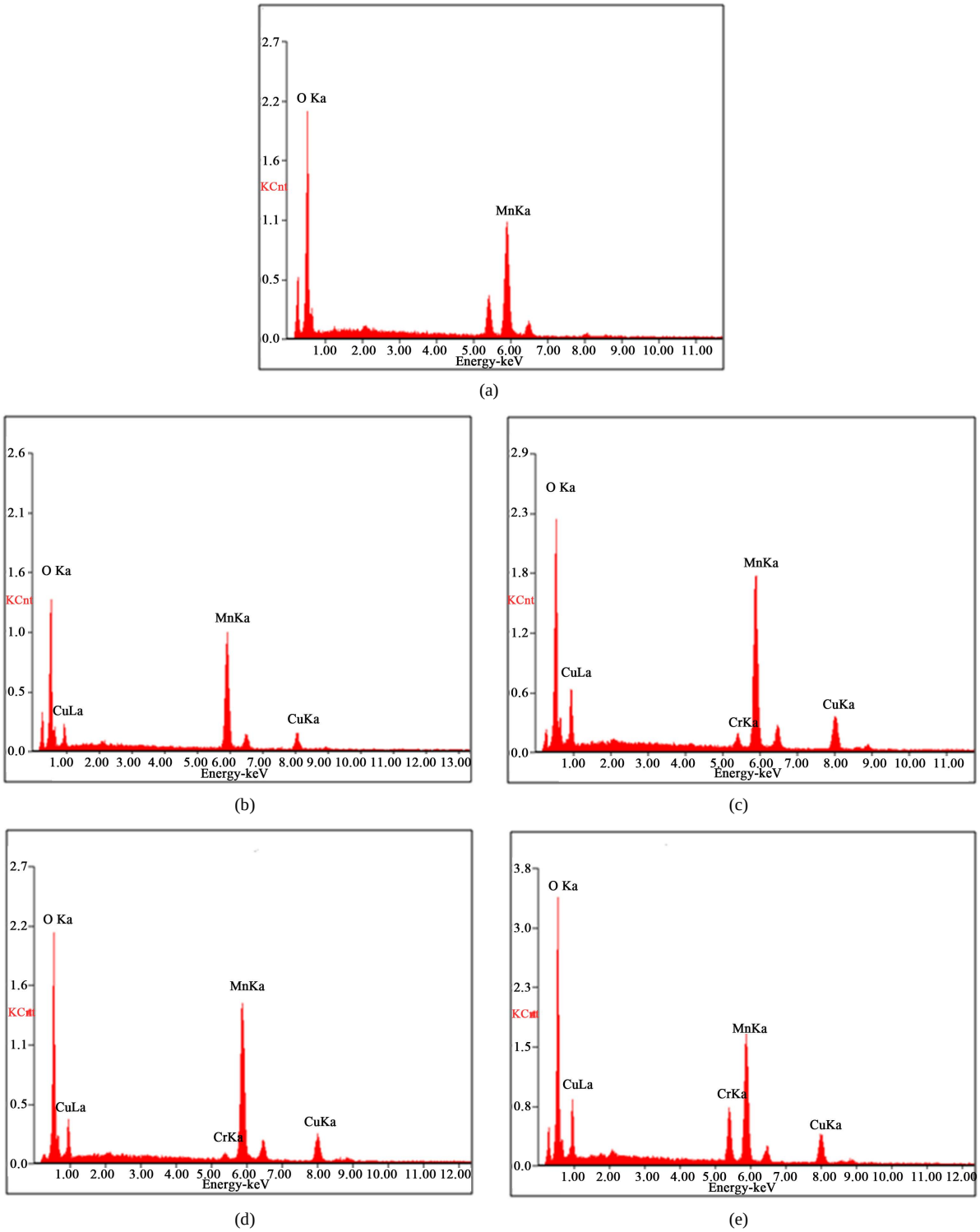


**Figure 9.** EDAX images of $LiMn_2O_4$ and $LiCu_xCr_vMn_{2-x-v}O_4$ powders calcined at 850˚C. (a) Undoped; (b) x = 0.50; (c) x = 0.50; y = 0.05; (d) x = 0.50; y = 0.10; (e) x = 0.50; y = 0.50.

cathodic efficiency of 88% corresponds to 94% columbic efficiency during the first cycle. It is evident to note that the undoped spinel exhibits superior performance to other doped spinels ($LiCu_xCr_yMn_{2-x-y}O_4$). Moreover, undoped spinel has been derived via sol-gel method [30] and delivers the maximum discharge capacity of 125

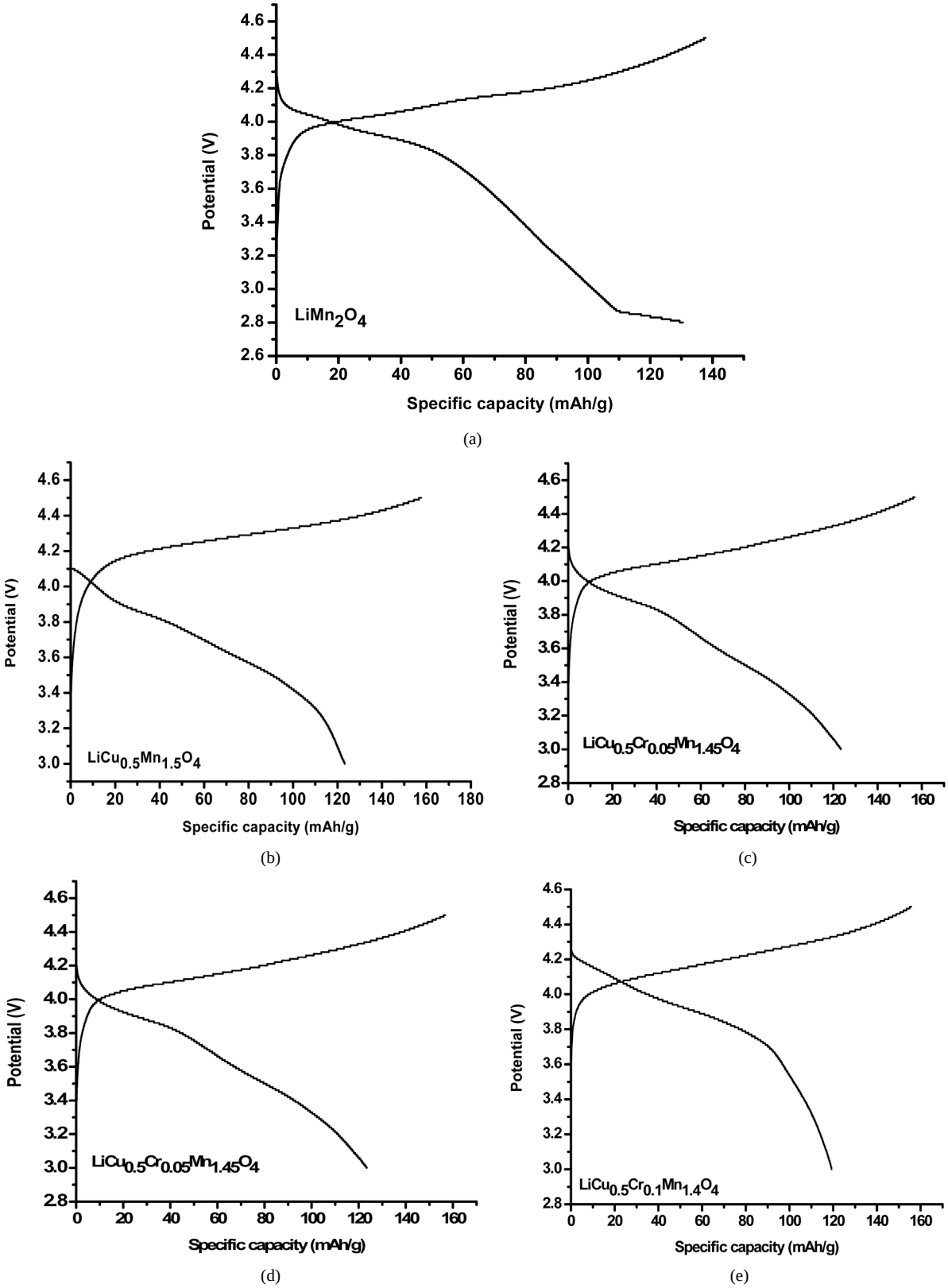


**Figure 10.** First cycle charge-discharge behaviour of $LiMn_2O_4$ and $LiCu_xCr_yMn_{2-x-y}O_4$. (a) Undoped; (b) $x = 0.50$; (c) $x = 0.50$; $y = 0.05$; (d) $x = 0.50$; $y = 0.10$; (e) $x = 0.50$; $y = 0.50$.

mA·h/g during the first cycle in which these results showing inferior performance to our present investigation. Similarly, another pristine $LiMn_2O_4$ has been synthesized through sol-gel method offers an initial reversible capacity of 128 mA·h/g [31] wherein it seems to be lower than our result. Also, copper doped spinel has been attempted to synthesize via sol-gel method [32] and delivers the maximum discharge of capacity of 128 mA·h/g during the first cycle. These experiment results are slightly lower than to our present report. Nevertheless, during sol-gel synthesis of spinel compounds, Myristic acid has been used as chelating agent to be favorable and to act as catalyst to fasten the reaction causing the multi-ligand chain between Mn-O and $COO^-$ resulting in the formation of pristine $LiMn_2O_4$ and $LiCu_xCr_yMn_{2-x-y}O_4$ for augmenting the high electrochemical stability of the spinel compound.

**Figures 10(b)-(e)** show the first cycle charge-discharge behavior of $LiCu_xCr_yMn_{2-x-y}O_4$ heated at 850˚C. Copper and copper-chromium doped spinels exhibit the discharge capacity of 122, 124, 120 and 120 mA·h/g corresponds to 77%, 78%, 77% and 76% columbic efficiency during the first cycle (**Figures 10(b)-(e)**). It is quite interesting to note that 0.5-Cu doped spinel has been experimented to synthesize through sol-gel route [32] and yields the maximum discharge capacity of 70 mA·h/ g in the first cycle. It shows the poor performance rather than our results. Similarly, 0.05-$Cr^{3+}$ modified $LiMn_2O_4$ spinel intercalation cathodes through oxalic acid assisted sol-gel method for lithium rechargeable batteries has been reported [24] and exhibits an initial discharge capacity of 80 mA·h/g wherein these results are lower than that of our present performance. It is well known that the sample with low Cr-doping ($LiCu_{0.5}Cr_{0.05}Mn_{1.45}O_4$) exhibits the higher discharge capacity (124 mA·h/g) than the other all slightly high doping compositions. The increase in capacity may be due to the same oxidation state of chromium ions have smaller ionic radii than manganese ions, $Cr^{3+}$ (0.615 Å), $Mn^{3+}$ (0.68 Å), $Cr^{4+}$ (0.58 Å), $Mn^{4+}$ (0.60 Å). Also the stronger Cr-O bonds in the delithiated state (compare the binding energy of 1142 kJ·mol$^{-1}$ for $CrO_2$ with 946 kJ mol$^{-1}$ for $\alpha$-$MnO_2$) may also be considered to contribute to stabilization energy of $Cr^{3+}$ in the octahedral sites. Therefore, the equal doping ratio of spinel ($LiCu_{0.5}Cr_{0.5}Mn_{1.0}O_4$) delivers slightly lower performance (discharge capacity of 120 mA·h/g) than undoped and other dopant compositions may be owing to high order of cationic mixing of dopants, poor electronic conductivity, and higher electrochemical impedance has been developed inside the cell which is reflected in electrochemical impedance spectra (ECI).

The cycling behavior of undoped and doped spinels calcined at 850˚C over investigated 10 cycles with the corresponding columbic efficiencies (CE) is shown in **Figures 11(a)-(e)**. The undoped spinel exhibits the maximum discharge capacity of 130 mA·h/g in the first cycle. However, it besets from capacity fading drastically upon cycling up to 10 cycles and also it experiences a capacity fade of 1.4 mA·h/g cycle over the investigated 10 cycles with capacity retention of 89%. In the 5$^{th}$ and 10$^{th}$ cycle, the undoped spinel delivers a discharge capacity of 125, 116 mA·h/g or both same columbic efficiency of 99%. Similarly, the cells with copper and copper-chromim doped spinels deliver the discharge capacities of 123, 124, 120 and 120 mA·h/g during the first cycle and experiencing a capacity fade of 1.1, 1.1, 1.2 and 1.4 mA·h/g cycle with capacity retention of 92, 90, 91 and 88% for the Cu and Cu:Cr contents corresponding to 0.5, 0.5; 0.05, 0.5; 0.10 and 0.50; 0.50, respectively over the investigated 10 cycles. In the 5$^{th}$ and 10$^{th}$ cycle of doped spinels, the discharge capacities have been exhibited 118, 112; 115, 111; 112, 109; 114, 106 mA·h/g; with capacity fades of 0.1, 0.2; 0.1, 0.1; 0.1, 0.1; 0.1, 0.2 mA·h/g cycle corresponding to columbic efficiency of 99v, 98%; 99%, 99%; 99%, 99%; 99%, 98% for the Cu and Cu:Cr contents with regard to 0.5, 0.5:0.05, 0.5:0.10 and 0.50:0.50, respectively. Inter alia all dual doped compositions, the low Cr-doped spinels ($LiCu_{0.5}Cr_{0.05}Mn_{1.45}O_4$) offers better stable capacity retention up to 10 cycles. Several researchers have already reported [33] that 0.2-Cr doped $LiMn_2O_4$ has been synthesized by sol-gel method as cathodes in high-voltage lithium batteries and delivered the maximum discharge capacity of 78 mA·h/gin the 10$^{th}$ cycle. These results are not encouraging and inferior to our present investigation (109 mA·h/g). Also, 0.01-Cr doped spinel has been synthesized towards intercalation cathodes through oxalic acid assisted sol-gel method for lithium rechargeable batteries and delivers the inferior results of discharge capacity of 115 mA·h/g in the 10$^{th}$ cycle [24] when compare to our present investigation. Moreover, 0.01-Cr doped pristine spinel has also been prepared using Adipic acid as chelating agent via sol–gel route and exhibits the maximum discharge capacity of 117 mA·h/g in the 10$^{th}$ cycle [23] wherein these results are found to be somewhat lower in our earlier experiment rather than this work. In other words, 0.5-Cu doped spinel has been reported via sol-gel method [32] and delivers the maximum discharge capacity of 60 mA·h/g in the 10$^{th}$ cycle which is two times lower than our results. Moreover, 0.1-Al doped spinel has been experimented via traditional sol-gel method [34] exhibits 100 mA·h/g in the 10$^{th}$ cycle sans stable discharge capacity wherein these results are lower

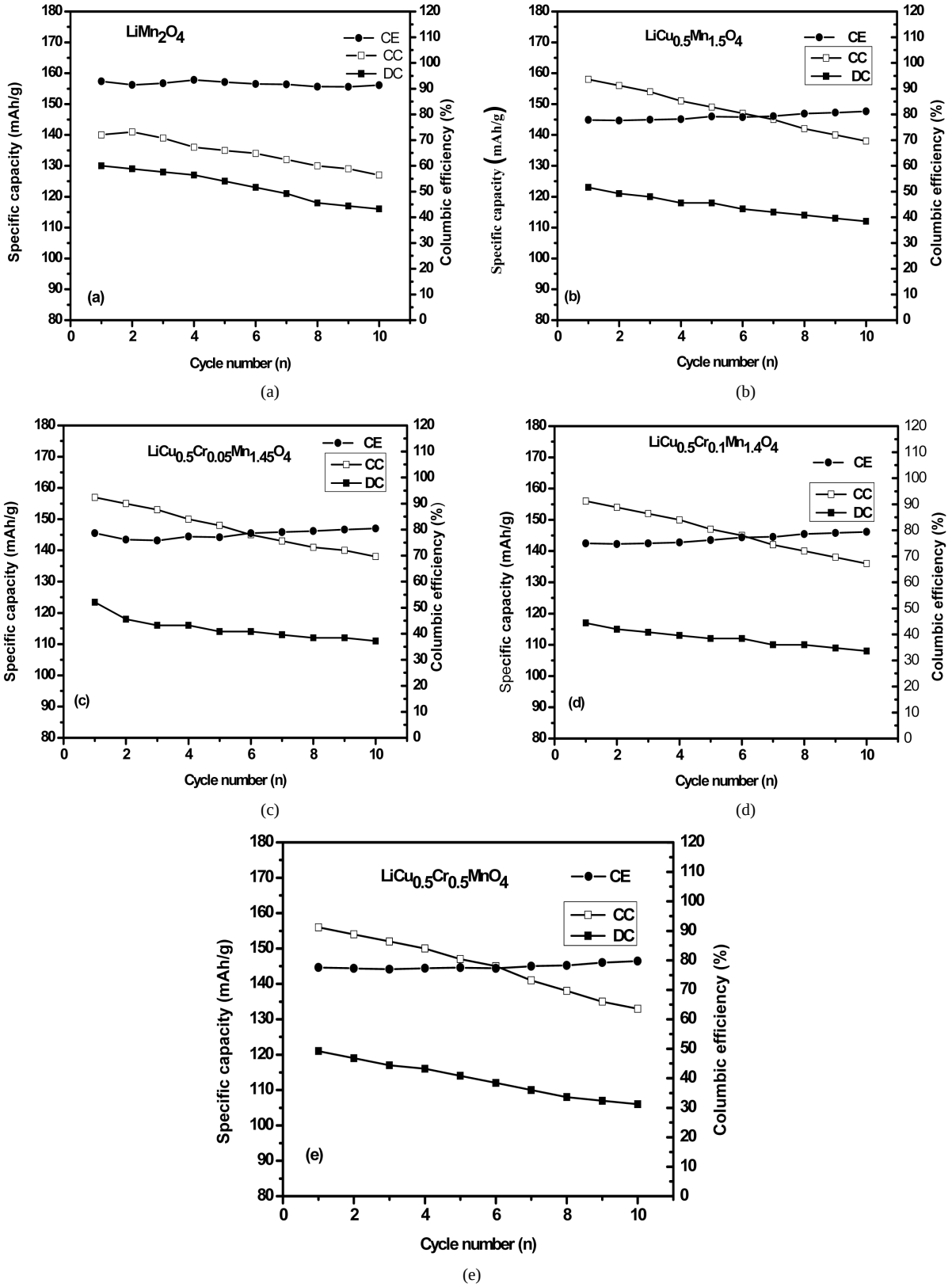


**Figure 11.** Cycling behaviour of $LiMn_2O_4$ and $LiCu_xCr_vMn_{2-x-v}O_4$. (a) Undoped; (b) x = 0.50; (c) x = 0.50; y = 0.05; (d) x = 0.50; y = 0.10; (e) x = 0.50; y = 0.50.

than our reported investigation (106 mA·h/g) with good capacity retention. It is quite interesting to know the discharge capacities of pristine spinels synthesized by different methods suggesting that 0.1-Cr doped spinel synthesizes via green chemistry method/sol-gel method and delivers the specific discharge capacity of 95 mA·h/g in the 10$^{th}$ cycle [24]. These results are not superior to our present work. Hence, it is concluded from the charge-discharge and cycling studies that among all dual doped spinels, the low amount of Cr-doped spinel ($LiCu_{0.5}Cr_{0.05}Mn_{1.45}O_4$) is an apt candidate to enhance the electrochemical stability of the spinel owing to higher octahedral stabilization energy of $Cr^{3+}$ (1142 kJ·mole$^{-1}$) as compared to that of manganese (946 kJ·mole$^{-1}$) and effect of chromium will be more pronounced in reducing the capacity fade leads to decrease in cell volume to augment the stability of the structure during the deintercalation/intercalation process. Thus, low chromium doped spinel ($LiCu_{0.5}Cr_{0.05}Mn_{1.45}O_4$) stabilizes the $Mn^{3+}$ structure for increasing good cycleability with better capacity retention. Also the stronger Cr-O bonds in the delithiated state (compare the binding energy of 1142 kJ·mol$^{-1}$ for $CrO_2$ with 946 kJ·mol$^{-1}$ for $\alpha$-$MnO_2$) may also be considered to contribute to stabilization energy of $Cr^{3+}$ in the octahedral sites.

## 3.8. Electrochemical Impedance Spectroscopy

**Figures 12(a)-(e)** show the Nyquist plot of electrochemical impedance spectra of (EIS) coin cells after 10 cycles. The Nyquist plots depict the single semicircle in the high frequency region and straight sloping line in the low frequency region. Such Nyquist plots are the relaxation frequency due to the interfacial polarization. All the Nyquist spectra depict the high-frequency semicircle with a maximum at a frequency of few kilo-ohms. This may be due to highly charged state and the typical behavior of the diffusion kinetic process inside the electrode materials. Also, having the high-frequency semicircle to the charge of the surface area of the spinel oxide positive electrodes. This real impedance belongs to both interparticle electronic contact and ionic diffusion via the passivation layer. It is clearly seen that among all the five compounds, $LiCu_{0.5}Cr_{0.05}Mn_{1.45}O_4$ shows low resistance of 190 Ohms while undoped spinel depicting the real impedance of 350 Ohms. Similarly, in the case of $LiCu_{0.5}Mn_{1.5}O_4$, $LiCu_{0.5}Cr_{0.1}Mn_{1.4}O_4$ provides higher resistance of 500 and 275 Ohms than that of $LiCu_{0.5}Cr_{0.05}Mn_{1.45}O_4$. Moreover, an equal amount of high doping pristine spinel ($LiCu_{0.5}Cr_{0.5}Mn_{1.0}O_4$) exhibits the high electrochemical polarization of 2000 Ohms which is seemed to be higher impedance relatively to all the dopants. During charging, Li/$LiCu_{0.5}Cr_{0.05}Mn_{1.45}O_4$ couple delivers very lower electrochemical polarization of 350 Ohms than that of undoped and all doped spinels for the sake of good kinetic reactions and good thermodynamics. Hence, among all dual doped spinels, the stable specific discharge capacity has been offered by the low Cr-doped spinel ($LiCu_{0.5}Cr_{0.05}Mn_{1.45}O_4$) may be due to the low order of electrochemical polarization/charge transfer resistance ($R_{ct}$) and better electronic conductivity with mitigating of $Mn^{3+}$ from $Mn^{4+}$ for high diffusion of lithium ions during intercalation and de-intercalation process. $LiCu_{0.5}Cr_{0.5}Mn_{1.0}O_4$ samples show higher electrochemical impedance as a consequence of increasing the charge transfer resistance and charge transfer of lithium ions on the surface of the electrodes which leads to capacity fading upon cycling (10 cycles). In view of the above, the impedance behaviour of 0.05-Cr doped spinel shows an excellent electrochemical performance.

## 3.9. dQ/dE vs. Potential Curves

The differential capacity curve of the parent $LiMn_2O_4$calcined at 850˚C is shown in **Figure 13(a)**. This curve depicts lucidly two redox peaks respectively. The oxidative peaks correspond to the extraction of lithium ions and reductive peaks are insertion of lithium ions. The first two predominant anodic peaks are seen at about 4.01 and 4.15 V corresponds to $Mn^{3+}/Mn^{4+}$ couples with an average oxidation state of 3.5 while another two well defined cathodic peaks appearing at around 3.98 and 4.1 V owing to the reductive behavior of the spinel. Moreover, these two anodic peaks of undoped spinel depict the high anodic peak currents at around 0.0018 and 0.00145 mA·h$^{g-1}$·mV$^{-1}$ with the cathodic peak currents of −0.00195 and −0.00194 mA·h$^{g-1}$·mV$^{-1}$. Hence, it is vindicated that the anodic process is more facile than cathodic one.

**Figure 13(b)** depicts the differential capacity cure of $LiCu_{0.5}Cr_{0.05}Mn_{1.45}O_4$ calcined at 850˚C. It is well known that two well defined anodic peaks are seen between 4.02 and 4.15 V attributed to the de-intercalation process with $Mn^{3+}/Mn^{4+}$, $Cu^{2+}/Cu^{3+}$ and $Cr^{3+}/Cr^{4+}$ couples respectively. Similarly, two anodic peaks of $LiCu_{0.5}Cr_{0.05}Mn_{1.45}O_4$ exhibit the high anodic peak currents at around 0.0065 and 0.002 mA·h$^{g-1}$·mV$^{-1}$ with the cathodic peak currents of −0.0045 and −0.0021 mA·h$^{g-1}$·mV$^{-1}$ at about 4.11 and 4 V. It is evident that the differential capacity curve of $LiCu_{0.5}Cr_{0.05}Mn_{1.45}O_4$ exhibits the better performance in both peak currents when

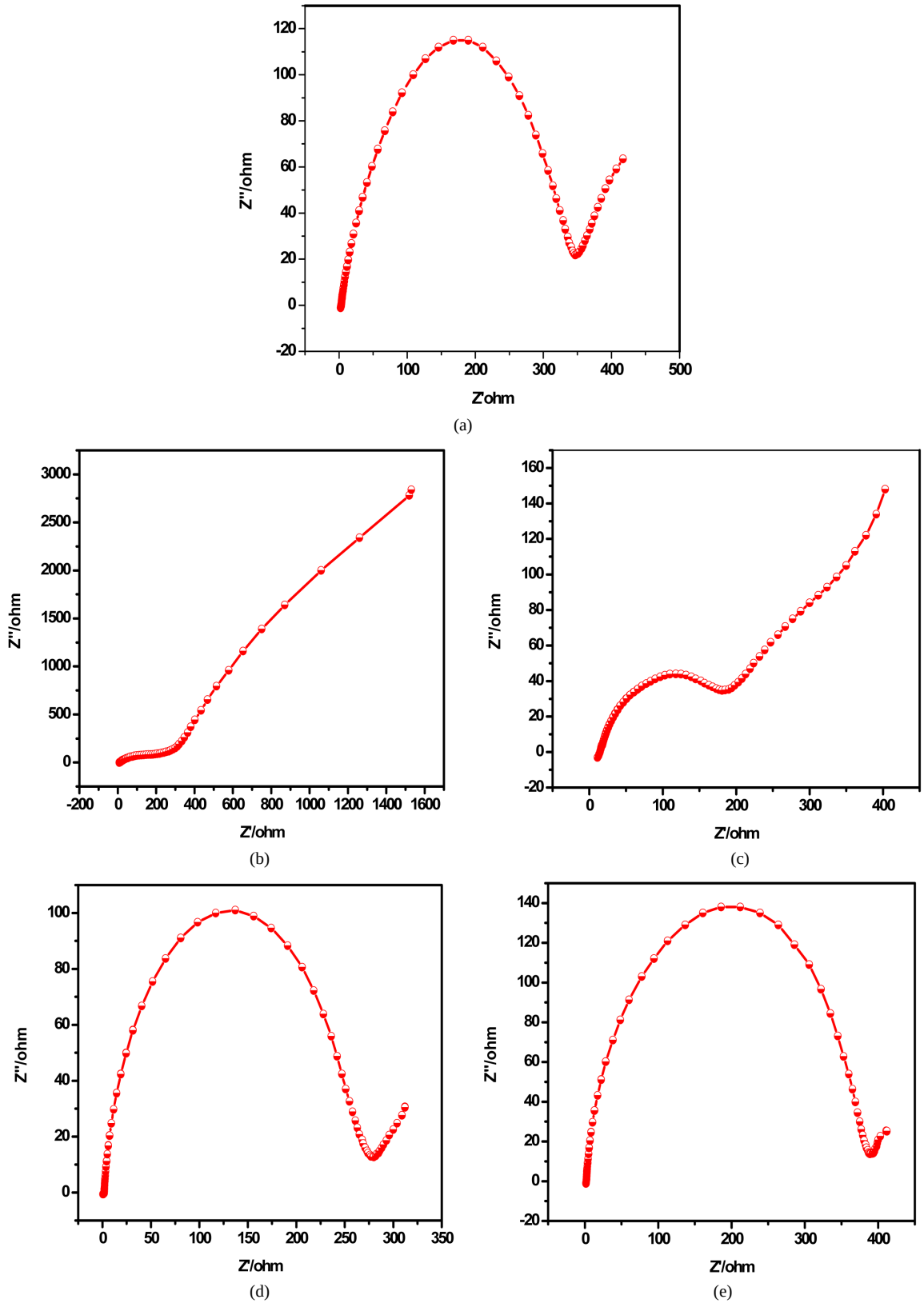


**Figure 12.** Electrochemical Impedance spectra (EIS) of the cells ($LiMn_2O_4$ and $LiCu_xCr_yMn_{2-x-y}O_4$) after 10 cycles. (a) Undoped; (b) x = 0.50; (c) x = 0.50; y = 0.05; (d) x = 0.50; y = 0.10; (e) x = 0.50; y = 0.50.

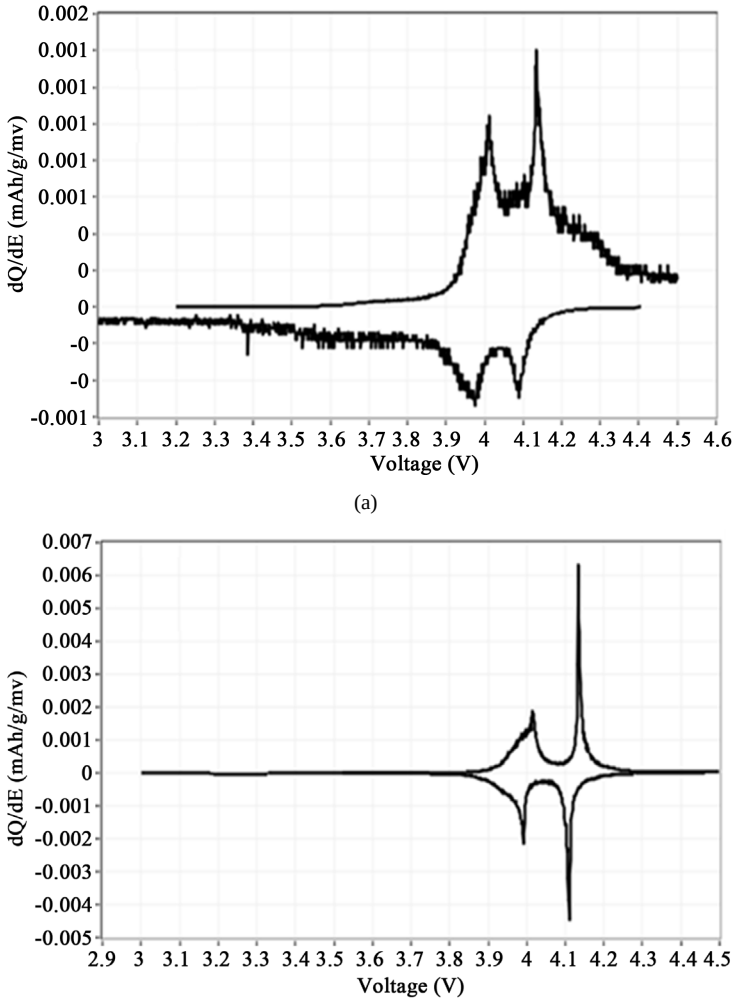


**Figure 13.** Differential capacity curves of (a) $LiMn_2O_4$; (b) $LiCu_{0.5}Cr_{0.05}Mn_{1.45}O_4$.

compared with undoped spinel. Hence, it is concluded that the low amount of chromium doped spinel ($LiCu_{0.5}Cr_{0.05}Mn_{1.45}O_4$) increases the electrochemical stability of the compound which has been reverberated in cycleability studies.

## 4. Conclusion

Pristine spinel $LiMn_2O_4$ and $LiCu_xCr_yMn_{2-x-y}O_4$ (x, y = Cu, Cr) (x = 0.50; y = 0.05 - 0.50) powders have been synthesized via sol-gel method for the first time using Myristic acid as the chelating agent to obtain micron sized particles for use as cathode materials in lithium rechargeable batteries. XRD patterns of $LiMn_2O_4$ and $LiCu_xCr_yMn_{2-x-y}O_4$ heated at 850˚C corroborate the high degree of crystallinity with better phase purity of synthesized materials via sol-gel synthesis. FESEM image of undoped pristine spinel lucidly reveals cauliflower morphology with good agglomerated particle size of 50 nm while 0.5-Cu doped samples depict the pebbles morphology. TEM images of the spinel $LiMn_2O_4$ and $LiCu_{0.5}Cr_{0.05}Mn_{1.45}O_4$ substantiate that all the synthesized particles via sol-gel method are nano-sized (100 nm) with spherical surface and cloudy particles morphology. EDAX peaks confirm their actual composition of Cu, Cr, Mn and O in $LiMn_2O_4$ and $LiCu_xCr_yMn_{2-x-y}O_4$. Electrochemical impedance spectroscopy (EIS) measurements of spinel $LiMn_2O_4$ and $LiCu_{0.5}Cr_{0.05}Mn_{1.45}O_4$ exhibit the high and low order of polarization of (350 and 190 Ohms) after 10 cycles. Among all dopant concentrations attempted, $LiCu_{0.5}Cr_{0.05}Mn_{1.45}O_4$ sample exhibits the best performance (1$^{st}$ cycle discharge capacity: 124 mA·h/g) with low capacity fade of 1.1 mA·h/g cycle and capacity retention of 90%.

## Acknowledgements

One of the authors Dr. R. Thirunakaran is thankful for the support given under the "Brain Pool Program of the Korean Federation of Science and Technology Societies" (KOFST), Republic of South Korea and also grateful to Prof. Won-Sub Yoon, for his help and valuable guidance. Further, Dr. R. Thirunakaran, thanks Dr. Vijayamohanan K. Pillai, Director, CSIR-CECRI for granting leave to avail the above fellowship. Also, this work was supported by the Human Resources Development Program (No. 20124010203270) of the Korea Institute of Energy Technology Evaluation and Planning (KETEP) grant funded by the Korea government Ministry of Trade, Industry and Energy. Many thanks are to the students of Professor for their co-operative helps and Cooperative Center for Research Facilities (CCRF) for completion of all physical characterization studies during my fellowship at Sungkyunkwan University (SKKU), South Korea.

## References

[1] Tarascon, J.M., McKinnon, W.R., Coowar, F., Bowner, T.N., Amatucci, G. and Guyomard, D. (1994) Synthesis Conditions and Oxygen Stoichiometry Effects on Lithium Insertion into the Spinel $LiMn_2O_4$. *Journal of the Electrochemical Society*, **141**, 1421-1431. http://dx.doi.org/10.1149/1.2054941

[2] Gummow, R.J., de Kock, A. and Thackeray, M.M. (1994) Improved Capacity Retention in Rechargeable 4 V Lithium/Lithium-Manganese Oxide (Spinel) Cells. *Solid State Ionics*, **69**, 59-67. http://dx.doi.org/10.1016/0167-2738(94)90450-2

[3] Thackeray, M.M., de Kock, A., Rossouw, M.H., Liles, D., Bittihn, R. and Hoge, D. (1992) Spinel Electrodes from the Li-Mn-O System for Rechargeable Lithium Battery Applications. *Journal of the Electrochemical Society*, **139**, 363-366. http://dx.doi.org/10.1149/1.2069222

[4] Xia, Y., Zhou, Y. and Yoshio, M. (1997) Capacity Fading on Cycling of 4 V $Li/LiMn_2O_4$ Cells. *Journal of the Electrochemical Society*, **144**, 2593-2600. http://dx.doi.org/10.1149/1.1837870

[5] Pistoia, G., Antonini, A., Rosati, R. and Zane, D. (1996) Storage Characteristics of Cathodes for Li-Ion Batteries. *Electrochimca Acta*, **41**, 2683-2689. http://dx.doi.org/10.1016/0013-4686(96)00122-3

[6] Jang, D.H., Shin, J.Y. and Oh, S.M. (1996) Dissolution of Spinel Oxides and Capacity Losses in 4 V $Li/Li_xMn_2O_4$ Cells. *Journal of the Electrochemical Society*, **143**, 2204-2211. http://dx.doi.org/10.1149/1.1836981

[7] Yamada, A. (1996) Lattice Instability in Li $(Li_xMn_{2-x})O_4$. *Journal of Solid State Chemistry*, **122**, 160-165. http://dx.doi.org/10.1006/jssc.1996.0097

[8] Ohuzuku, T., Takeda, S. and Wakihara, M. (1999) Olivine Coated Spinel: 5 V System for High Energy Lithium Batteries. *Journal of Power Sources*, **90**, 81-82.

[9] Song, D., Ikuta, H., Uchida, T. and Wakihara, M. (1999) The Spinel Phases $LiAl_yMn_{2-y}O_4$ ($y$ = 0, 1/12, 1/9, 1/6, 1/3) and Li $(Al, M)_{1/6}$ $Mn_{11/6}O_4$ (M=Cr, Co) as the Cathode for Rechargeable Lithium Batteries. *Solid State Ionics*, **117**, 151-156. http://dx.doi.org/10.1016/S0167-2738(98)00258-6

[10] Iqbal, M.J. and Ahmad, Z. (2008) Electrical and Dielectric Properties of Lithium Manganate Nanomaterials Doped with Rare-Earth Elements. *Journal of Power Sources*, **179**, 763-769. http://dx.doi.org/10.1016/j.jpowsour.2007.12.115

[11] Lee, J.H., Hong, J.K., Jang, D.H., Sun, Y.K. and Oh, S.M. (2000) Degradation Mechanisms in Doped Spinels of $LiM_{0.05}Mn_{1.95}O_4$ (M = Li, B, Al, Co, and Ni) for Li Secondary Batteries. *Journal of Power Sources*, **89**, 7-14. http://dx.doi.org/10.1016/S0378-7753(00)00375-X

[12] Park, S.H., Park, K.S., Sun, Y.K. and Nahm, K.S. (2000) Synthesis and Characterization of a New Spinel, $Li_{1.02}Al_{0.25}Mn_{1.75}O_3S_{0.03}$, Operating at Potentials between 4.3 and 2.4 V. *Journal of Electrochemical Society*, **147**, 2116-2121. http://dx.doi.org/10.1149/1.1393494

[13] Bach, S., Henry, M., Baffier, N. and Livage, J. (1990) Sol-Gel Synthesis of Manganese Oxide. *Journal of Solid State Chemistry*, **88**, 325-333. http://dx.doi.org/10.1016/0022-4596(90)90228-P

[14] Perreira-Ramos, J.P. (1995) Electrochemical Properties of Cathodic Materials Synthesized by Low-Temperature Techniques. *Journal of Power Sources*, **54**, 120-126. http://dx.doi.org/10.1016/0378-7753(94)02051-4

[15] Barboux, P., Tarascon, J.M. and Shokoohi, F.K. (1991) The Use of Acetates as Precursors for the Low Temperature Synthesis of $LiMn_2O_4$ and $LiCoO_2$ Intercalation Compounds. *Journal of Solid State Chemistry*, **94**, 185-196. http://dx.doi.org/10.1016/0022-4596(91)90231-6

[16] Liu, W., Farrington, G.C., Chaput, F. and Dunn, B.J. (1996) Synthesis and Electrochemical Studies of Spinel Phase $LiMn_2O_4$ Cathode Materials Prepared by the Pechini Process. *Journal of Electrochemical Society*, **143**, 879-884. http://dx.doi.org/10.1149/1.1836552

[17] Thirunakaran, R., Kalaiselvi, N., Periasamy, P., RameshBabu, B., Renganathan, N.G. and Muniyandi, N. (2001) Signi-

ficance of Mg Doped $LiMn_2O_4$ Spinels as Attractive 4 V Cathode Materials for Use in Lithium Batteries. *Ionics*, **7**, 187-191. http://dx.doi.org/10.1007/BF02419227

[18] Guo, S.H., Zhang, S.C., He, X.M., Pu, W.H., Jiang, C.Y. and Wan, C.R. (2008) Synthesis and Characterization of Sn-Doped $LiMn_2O_4$ Cathode Materials for Rechargeable Li-Ion Batteries. *Journal of the Electrochemical Society*, **155**, A760-A763. http://dx.doi.org/10.1149/1.2965635

[19] Thirunakaran, R., Sivashanmugam, A., Gopukumar, S., Dunnill, C.W. and Gregory, D.H. (2008) Electrochemical Behaviour of Nano-Sized Spinel $LiMn_2O_4$ and $LiAl_xMn_{2-x}O_4$ ($x$ = Al: 0.00 - 0.40) Synthesized via Fumaric Acid-Assisted Sol-Gel Synthesis for Use in Lithium Rechargeable Batteries. *Journal of Physics Chemistry of Solids*, **69**, 2082-2090. http://dx.doi.org/10.1016/j.jpcs.2008.03.009

[20] Veluchamy, A., Ikuta, H. and Wakihara, M. (2001) Boron-Substituted Manganese Spinel Oxide Cathode for Lithium Ion Battery. *Solid State Ionics*, **143**, 161-171. http://dx.doi.org/10.1016/S0167-2738(01)00856-6

[21] Fey, G.T.K., Lu, C.Z. and Prem Kumar, T. (2003) Solid-State Synthesis and Electrochemical Characterization of $Li-M_yCr_{0.5-y}Mn_{1.5}O_4$ (M = Fe or Al; $0.0 < y < 0.4$) Spinels. *Materials Chemistry and Physics*, **80**, 309-318. http://dx.doi.org/10.1016/S0254-0584(02)00522-9

[22] Thirunakaran, R., Sivashanmugam, A., Gopukumar, S. and Rajalakshimi, R. (2009) Cerium and Zinc: Dual-Doped $LiMn_2O_4$ Spinels as Cathode Material for Use in Lithium Rechargeable Batteries. *Journal of Power Sources*, **187**, 565-574. http://dx.doi.org/10.1016/j.jpowsour.2008.10.134

[23] Thirunakaran, R., Kim, K.T., Kang, Y.M., Seo, C.Y. and Lee, J.Y. (2004) Adipic Acid Assisted Sol-Gel Route for Synthesis of $LiCr_xMn_{2-x}O_4$ Cathode Material. *Journal of Power Sources*, **137**, 100-104. http://dx.doi.org/10.1016/j.jpowsour.2004.02.016

[24] Thirunakaran, R., Kim, K.T., Kang, Y.M. and Lee, J.Y. (2005) $Cr^{3+}$ Modified $LiMn_2O_4$ Spinel Intercalation Cathodes through Oxalic Acid Assisted Sol-Gel Method for Lithium Rechargeable Batteries. *Materials Research Bulletin*, **40**, 177-186. http://dx.doi.org/10.1016/j.materresbull.2004.08.013

[25] Thirunakaran, R., Sivashanmugam, A., Gopukumar, S., Dunnill, C.W. and Gregory, D.H. (2008) Studies on Chromium/Aluminium Doped Managanese Spinel as Cathode Materials for Lithium-Ion Batteries—A Novel Chelated Sol-Gel Synthesis. *Journal of Materials Process & Technology*, **208**, 520-531. http://dx.doi.org/10.1016/j.jmatprotec.2008.01.017

[26] Thirunakaran, R., Sivashanmugam, A., Gopukumar, S., Dunnill, C.W. and Gregory, D.H. (2008) Phthalic Acid Assisted Nano-Sized Spinel $LiMn_2O_4$ and $LiCr_xMn_{2-x}O_4$($x$=0.00−0.40) via Sol-Gel Synthesis and Its Electrochemical Behaviour for Use in Li-Ion-Batteries. *Materials Research Bulletin*, **43**, 2119-2129. http://dx.doi.org/10.1016/j.materresbull.2007.09.021

[27] Penga, C., Huanga, J., Guoa, Y., Lia, Q., Baia, H., Hea, Y., Sua, C. and Guao, J. (2015) Electrochemical Performance of Spinel $LiAl_xMn_{2-x}O_4$ Prepared Rapidly by Glucose-Assisted Solid-State Combustion Synthesis. *Vacuum*, **120**, 121-126. http://dx.doi.org/10.1016/j.vacuum.2015.07.001

[28] Rajakumar, S., Thirunakaran, R., Sivashanmugam, A. and Gopukumar, S. (2010) Synthesis, Characterization, and Electrochemical Properties of $LiCr_xNi_yMn_{2-x-y}O_4$ Spinels as Cathode Material for 5 V Lithium Battery. *Journal of Electrochemical Society*, **157**, A333-A339. http://dx.doi.org/10.1149/1.3283015

[29] Julien, C., Mangani, I.R., Selladurai, S. and Massot, M. (2002) Synthesis, Structure and Electrochemistry of $LiMn_{2-y}Cr_{y/2}Cu_{y/2}O_4$ ($0.0 \leq y \leq 0.5$) Prepared by Wet Chemistry. *Solid State Ionics*, **4**, 1031-1038. http://dx.doi.org/10.1016/s1293-2558(02)01357-2

[30] Lu, C.H., Lin, Y.L. and Wang, H.C. (2003) Chromium-Ion Doped Spinel Lithium Manganate Nanoparticles Derived from the Sol-Gel Process. *Journal of Material Science Letters*, **22**, 615-618. http://dx.doi.org/10.1023/A:1023358731547

[31] Sun, Y.K, Oh, I.H. and Kim, K.Y. (1997) Synthesis of Spinel $LiMn_2O_4$ by the Sol-Gel Method for a Cathode-Active Material in Lithium Secondary Batteries. *Industrial and Engineering Chemistry Research*, **36**, 4839-4846. http://dx.doi.org/10.1021/ie970227b

[32] Murali, K.R., Saravanan, T. and Jeyachandran, M. (2008) Synthesis and Characterization of Copper Substituted Lithium Manganate Spinels. *Journal of Materials Science*: *Materials in Electronics*, **19**, 533-537. http://dx.doi.org/10.1007/s10854-007-9376-4

[33] Hernán, L., Morales, J., Sánchez, L. and Santos, J. (1999) Use of Li-M-Mn-O [M=Co, Cr, Ti] Spinels Prepared by a Sol-Gel Method as Cathodes in High-Voltage Lithium Batteries. *Solid State Ionics*, **118**, 179-185. http://dx.doi.org/10.1016/S0167-2738(98)00449-4

[34] Bao, S.J., Liang, Y.Y., Zhou, W.J., He, B.L. and Li, H.H. (2006) Synthesis and Electrochemical Properties of $Li-Al_{0.1}Mn_{1.9}O_4$ by Microwave-Assisted Sol-Gel Method. *Journal of Power Sources*, **154**, 239-245. http://dx.doi.org/10.1016/j.jpowsour.2005.03.220